17th AIAA/CEAS Aeroacoustics Conference (32nd AIAA Aeroacoustics Conference)
05 - 08 June 2011, Portland, Oregon
AIAA 2011-2835

Wavepacket Modeling of the Jet Noise Source

Dimitri Papamoschou*
University of California, Irvine, CA 92697, USA

This research is motivated by the need for physical models for the jet noise source to be used in practical noise prediction schemes for propulsion-airframe integration concepts. The emphasis is on jets with high-subsonic velocities typical of modern turbofan engines. The basis for the source model is an amplitude-modulated traveling wave - the wavepacket. Its parameters are determined by minimizing the difference between the modeled and experimental sound intensity distributions in the far field. Even though the pressure signal that reaches the far field is highly filtered, sufficient information is available to construct a wavepacket with reasonable physical characteristics. A simple stochastic extension of this concept shows a connection between the shape of the far-field sound pressure level spectrum and the emission polar angle. It suggests that the broadening of the spectrum with increasing polar angle can be explained on the basis of a single noise source (the wavepacket), rather than the prevailing model of two disparate noise sources, one coherent and the other incoherent.

I. Introduction

An increasing number of aerospace applications require physical modeling of the jet noise source. These include diffraction of jet noise from airframe surfaces, carrier deck noise, and rocket acoustics. Even though the jet noise source, and resulting emission, can be computed from first principles, such computations are very expensive and time consuming. What is sought here is a simple source model that captures the salient physics of the flow and reproduces faithfully the acoustic field. Further, the acoustic data used to calibrate and validate the model could be limited. For example, in the development of next-generation ANOPP tools for aircraft noise prediction, the only available data for determining the jet noise source are far-field autospectra at a range of polar and azimuth angles[1]. For subsonic jets, the information propagated to the far field is very limited, which presents a challenge in this type of determination of the noise source.

The intention of this paper is to develop approaches for determination of a physically meaningful jet noise source model based on the minimal information propagated to the far field. The principal component of this approach is the wavepacket model, i.e., an amplitude-modulated traveling wave of pressure prescribed on a near-field cylindrical surface. It is shown that the information propagated to the far field may be sufficient to estimate not only the overall shape of the wavepacket but also the content of its dominant azimuthal (helical) modes. In particular, a strong connection is made between the directivity of jet noise and the azimuthal mode content of the source. The wavepacket concept is extended to three-dimensional jets and to jets with limited azimuthal coherence.

An additional aspect of this study is re-examination the commonly held belief that the broadening of the sound pressure level (SPL) spectrum with increasing polar angle from the jet axis indicates two distinct noise sources, a "coherent" source radiating a small angles, and an "incoherent" source and radiating at large angles. This concept has found wide acceptance in the aerocoustic community. An overview its rationale can be found in Ref. 2. Indeed, there is significant circumstantial evidence to support the two-source model. On other hand, there is no conclusive proof that the turbulent jet has two distinct, independent, noise sources.

In this paper we adopt a holistic view of the far-field spectrum, in the form of a contour map on the Strouhal number (Sr) - polar angle (θ) plane. This is done in Fig.1 for a Mach 0.9 cold air jet. We note that the peak SPL level occurs at small angles and Sr~0.1. Plotted against frequency, the spectrum is

* Professor, Department of Mechanical and Aerospace Engineering, dpapamos@uci.edu, AIAA Fellow.

peaky at small polar angles and broader at large angles. The direction of peak emission increases considerably with increasing frequency, an important trend not scrutinized in previous works. Generally speaking, broadening of the spectrum indicates weaker temporal coherence of the acoustic field. Connecting this to the temporal or spatial coherence of the source is not straight-forward. A spatially-incoherent source field (e.g., a set of uncorrelated monoles) can generate an acoustic field with finite spatial coherence [3,4]. Further, we should allow for the possibility that the broadening of the spectrum with angle may be related to the propagation of sound from a distributed and directive source. Indeed, it will be shown that a single jet noise source model based on the wavepacket alone will capture the salient features of the spectrum of Fig.1.

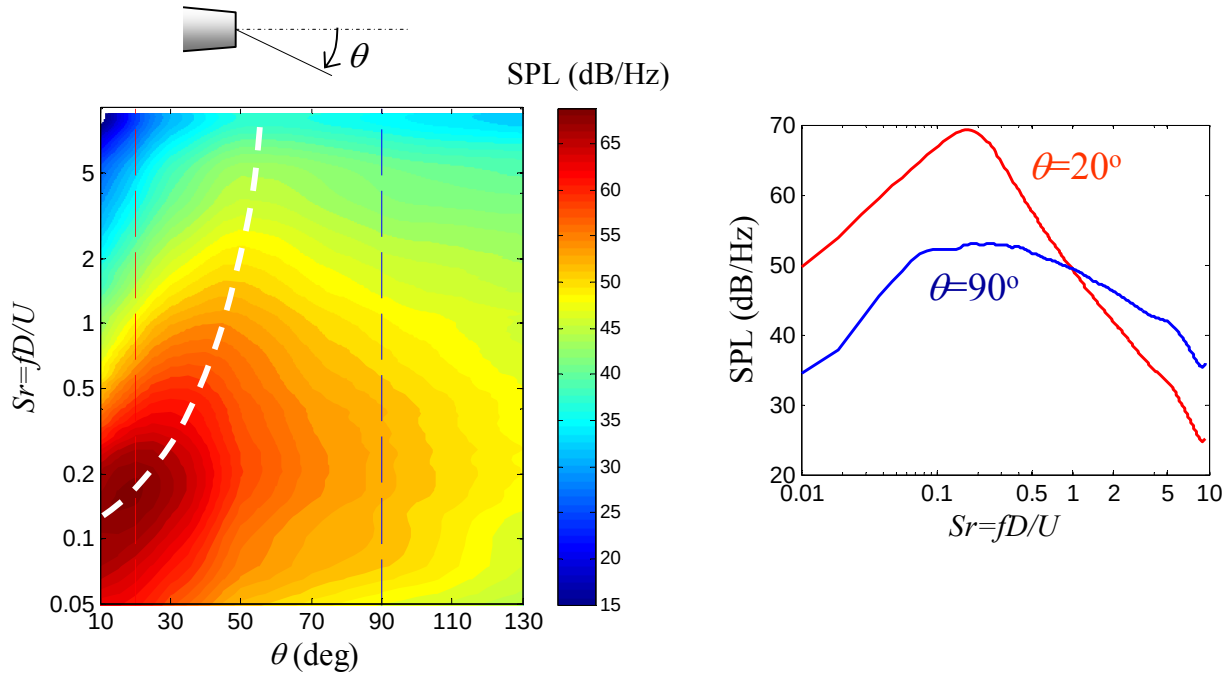

Fig. 1 Spectrum of the far-field sound pressure level for a Mach 0.9 cold jet. Contour map on the left plots the SPL versus polar angle and Strouhal number; white dashed line indicates polar direction of peak emission. Plot on the right shows the SPL versus Strouhal number at θ=20 and 90 deg.

The wavepacket model development of this paper builds on the foundational works by Tam and Burton[5], Crighton and Huerre[6], Avital *et al.*[7] and Morris[8]. There is increasing experimental evidence that the peak noise radiation is cause by an instability-wave mechanism, as evidenced by a number of near-field experiments, for example the works of Reba et al.[9,10]. Here we seek to understand and model the wavepacket noise source based on far-field intensity measurements, expanding on earlier related studies of our group[11].

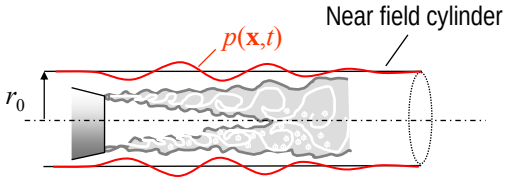

Fig. 2 Wavepacket concept.

Following the analysis by Morris[8], we consider a cylindrical surface surrounding a turbulent jet (Fig.2). The radius r_0 of the surface is sufficiently close to the jet to sense both the radiating and non-radiating (hydrodynamic) components of the turbulent pressure fluctuations. It is assumed that the cylinder is in a stationary ambient medium surrounding the jet.

The generic wavepacket model is depicted in Fig.3 and the coordinate systems used in the analysis that follows are shown in Fig.4. The paper starts with a deterministic noise source model based on the wavepacket ansatz. The model is then generalized to a stochastic perturbation. The test flow is a cold round air jet with Mach number M_j=0.9 and velocity U_j=285 m/s. The frequency f is presented in the non-dimensional form of Strouhal number $Sr=fD_j/U_j$.

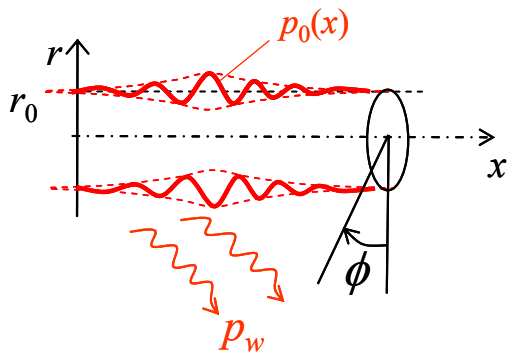

Fig. 3 Wavepacket model of jet noise.

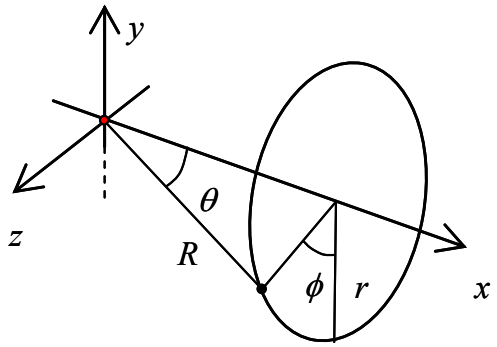

Fig. 4 Cartesian (x, y, z) , polar (x ,r, ϕ), and spherical (R, θ, ϕ) coordinate systems.

II. Deterministic Source Model

A. Elementary Model

On the cylinder surface $r=r_0$ we prescribe the pressure perturbation

$$p_w(n,r_0,x,\varphi,t) = p_0(x)e^{-i\omega t+in\phi} \tag{1}$$

where n denotes the azimuthal mode and ϕ is the azimuthal angle. The shape $p_0(x)$ takes the form $p_0(x) = A(x)e^{i\alpha x}$, with $A(x)$ an amplification-decay envelope that represents the axial coherence length scale, and α the wavenumber. Denoting the spatial Fourier transform of $p_0(x)$ as $\hat{p}_0(k)$, the solution for $r \geq r_0$ is[8]

$$p_w(n,r,x,\varphi,t) = \frac{1}{2\pi}e^{-i\omega t+in\phi}\int_{-\infty}^{\infty}\hat{p}_0(k)\frac{H_n^{(1)}(\lambda r)}{H_n^{(1)}(\lambda r_0)}e^{ikx}dk$$
$$\lambda = \left[\left(\frac{\omega}{a_\infty}\right)^2 - k^2\right]^{1/2}, \quad -\frac{\pi}{2} < \arg(\lambda) < \frac{\pi}{2} \tag{2}$$

where $H_n^{(1)}$ is the Hankel function of the first kind of order n. Equation 2 is the exact solution to the linearized problem, valid everywhere for $r \geq r_0$. An important aspect of the pressure field generated by the wavepacket is that it has a radiative (supersonic) component and a decaying (subsonic) component. It is useful to separate the two in order to gain insights into the mechanisms of diffraction. The decaying component involves phase speeds that are subsonic, $|\omega/k|<a_\infty$ or $|k|>\omega/a_\infty$:

$$p_{w,sub}(n,r,x,\varphi,t)=\frac{1}{2\pi}e^{-i\omega t+in\phi}\int_{|k|>\omega/a_\infty}\hat{p}_0(k)\frac{H_n^{(1)}(\lambda r)}{H_n^{(1)}(\lambda r_0)}e^{ikx}dk \tag{3a}$$

The radiating component involves phase speeds that are sonic or supersonic, $|k|\leq \omega/a_\infty$:

$$p_{w,\sup}(n,r,x,\varphi,t)=\frac{1}{2\pi}e^{-i\omega t+in\phi}\int_{-\omega/a_\infty}^{\omega/a_\infty}\hat{p}_0(k)\frac{H_n^{(1)}(\lambda r)}{H_n^{(1)}(\lambda r_0)}e^{ikx}dk \tag{3b}$$

From Eq.3b, using the convolution property of the Fourier transform, we obtain an expression for the part of $p_0(x)$ that radiates to the far field:

$$p_{0,\sup}(x)=\frac{1}{\pi}\int_{-\infty}^{\infty}\frac{p_0(\xi)}{x-\xi}\sin\left[\frac{\omega}{a_\infty}(x-\xi)\right]d\xi \tag{4}$$

The far-field approximation of Eq.2 is[8]

$$p_{w,far}(n,R,\theta,\varphi,t)=-\frac{i}{\pi R}\frac{\hat{p}_0\left(\frac{\omega}{a_\infty}\cos\theta\right)}{H_n^{(1)}\left(\frac{\omega}{a_\infty}r_0\sin\theta\right)}e^{i\omega R/a_\infty}e^{-i\omega t+in\phi} \tag{5}$$

where R is the distance of the observer from the origin and θ is the polar angle from the downstream wavepacket (jet) axis. The modulus squared of Eq.5 yields the modeled intensity of the far-field pressure:

$$S_{w,far}(n,R,\theta,\omega)=\frac{1}{(\pi R)^2}\left|\frac{\hat{p}_0\left(\frac{\omega}{a_\infty}\cos\theta\right)}{H_n^{(1)}\left(\frac{\omega}{a_\infty}r_0\sin\theta\right)}\right|^2 \tag{6}$$

B. Model with Azimuthal Amplitude Variation

We generalize the approach of Eq.1 by imposing an arbitrary azimuthal variation that can include the helical mode term $e^{in\phi}$ as well as an azimuthal amplitude variation. This approach is relevant to jets with non-axisymmetric noise source distribution and allows the development of a stochastic noise source model wherein the noise source has limited azimuthal coherence. On the cylinder surface we prescribe the pressure

$$p_w(r_0,x,\varphi,t)=p_0(x)G(\varphi)e^{-i\omega t} \tag{7}$$

where $G(\phi)$ is an azimuthal variation that can include helical modes and/or non-uniformities due to asymmetric flows. Expressing $G(\phi)$ in terms of its complex Fourier series

$$\begin{aligned}G(\varphi)&=\sum_{-\infty}^{\infty}g_m e^{im\varphi}\\ g_m&=\frac{1}{2\pi}\int_{-\pi}^{\pi}G(\varphi)e^{-im\varphi}d\varphi\end{aligned} \tag{8}$$

and denoting as before the spatial Fourier transform of $p_0(x)$ as $\hat{p}_0(k)$, the solution for $r\geq r_0$ is

$$p_w(r,x,\varphi,t)=\frac{1}{2\pi}e^{-i\omega t}\sum_{-\infty}^{\infty}g_m e^{im\varphi}\int_{-\infty}^{\infty}\hat{p}_0(k)\frac{H_{|m|}^{(1)}(\lambda r)}{H_{|m|}^{(1)}(\lambda r_0)}e^{ikx}dk$$
$$\lambda=\left[\left(\frac{\omega}{a_\infty}\right)^2-k^2\right]^{1/2},\qquad -\frac{\pi}{2}<\arg(\lambda)<\frac{\pi}{2} \tag{9}$$

The property $H_{-m}^{(1)}=(-1)^m H_m^{(1)}$ was used in deriving Eq.9. The same distinctions of radiative and decaying pressure fields hold as for the simple formulation. In other words, the decaying component involves phase speeds that are subsonic, $|k|>\omega/a_\infty$; the radiating component involves phase speeds that are sonic or supersonic, $|k|\le\omega/a_\infty$.

As an example, the azimuthal variation function $G(\phi)$ can take the forms of a Gaussian distribution or a square window function, both centered at ϕ_0, with width $\Delta\phi$ and helical mode n:

$$G(\varphi)=\exp\left[-18.42\left(\frac{\varphi-\varphi_0}{\Delta\varphi}\right)^2\right]e^{in\varphi}$$
$$G(\varphi)=\begin{Bmatrix}1, & |\varphi-\varphi_0|\le\Delta\varphi/2\\ 0, & |\varphi-\varphi_0|>\Delta\varphi/2\end{Bmatrix}e^{in\varphi} \tag{10}$$

For the Gaussian distribution, $\Delta\phi$ represents the 1% width.

Using the asymptotic form of the Hankel function

$$H_m^{(1)}(\zeta)\to\sqrt{\frac{2}{\pi\zeta}}\exp\left[i\left(\zeta-\frac{\pi}{4}-m\frac{\pi}{2}\right)\right],\quad |\zeta|\to\infty$$

the method of stationary phase gives the following result for the pressure in the far field:

$$p_{w,far}(R,\theta,\varphi,t)=-\frac{i}{\pi R}e^{i\omega R/a_\infty}e^{-i\omega t}\hat{p}_0\left(\frac{\omega}{a_\infty}\cos\theta\right)\sum_{m=-\infty}^{\infty}\frac{g_m e^{-i|m|\frac{\pi}{2}}}{H_{|m|}^{(1)}\left(\frac{\omega}{a_\infty}r_0\sin\theta\right)}e^{im\phi} \tag{11}$$

where R is the distance of the observer from the origin and θ is the polar angle from the downstream wavepacket (jet) axis. The modulus squared of Eq.11 yields the intensity of the far-field pressure:

$$S_{w,far}(R,\theta,\varphi,\omega)=\frac{1}{(\pi R)^2}\left|\hat{p}_0\left(\frac{\omega}{a_\infty}\cos\theta\right)\right|^2\left|\sum_{m=-\infty}^{\infty}\frac{g_m e^{-i|m|\frac{\pi}{2}}}{H_{|m|}^{(1)}\left(\frac{\omega}{a_\infty}r_0\sin\theta\right)}e^{im\phi}\right|^2 \tag{12}$$

Equation 12 is a generalization of Eq. 6 for a wavepacket with arbitrary azimuthal variation. It is evident that the azimuthal directivity (summation term on the right hand side) is independent of the wavepacket shape $p_0(x)$. This means that we can study the azimuthal spreading of a disturbance independently of the axial shape of the wavepacket.

We examine the propagation of an isolated azimuthal disturbance, as illustrated by the left diagram of Fig. 5. On the wavepacket surface we prescribe a disturbance with Gaussian azimuthal distribution (Eq.10, top) having 1% width of 30 deg. This is shown as the black line in Fig. 5. The colored lines represent the azimuthal distributions of the far-field intensity at different polar angles θ and at Strouhal number Sr=0.5. Note that all the intensity distributions have been normalized by their maximum values. The azimuthal spreading as the disturbance propagates to the far field is significant. Further insight is gained by the contour plots of Fig. 6 that depict the azimuthal spreading of a localized disturbance versus azimuthal and polar angles and for different Strouhal numbers. For Sr=0.1, the azimuthal spreading is

substantial and a disturbance prescribed at the bottom of the jet spreads toward the top of the jet. The spreading becomes progressively more confined with increasing frequency.

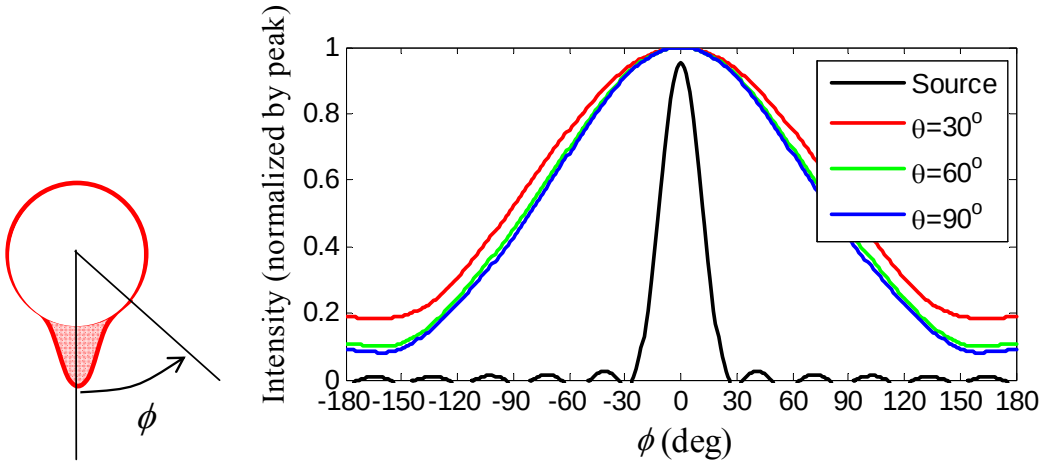

Fig. 5 Azimuthal spreading of a localized disturbance on the wavepacket surface.

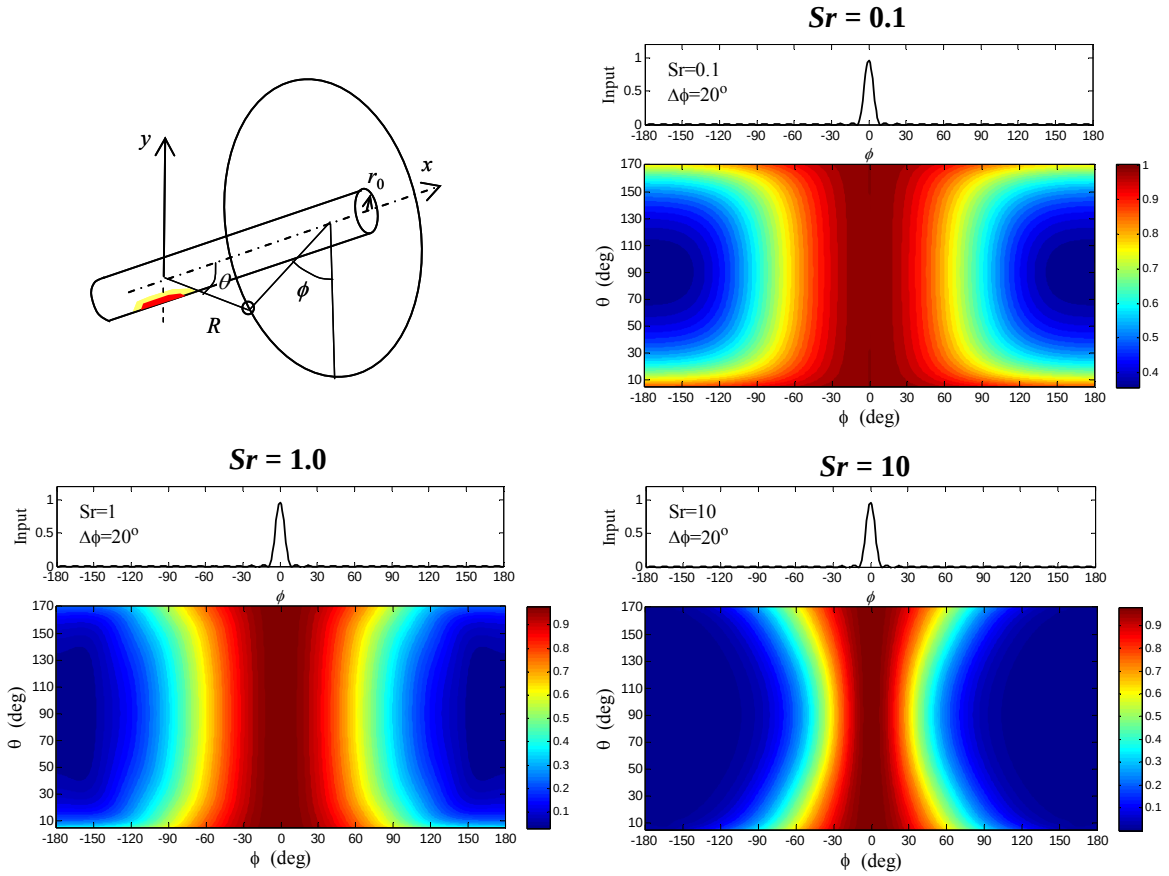

Fig. 6 Azimuthal spreading of a localized disturbance versus polar angle for various Strouhal numbers.

C. Self-Similar Model

This is a special implementation of the wavepacket model, applicable to the shear layer surrounding the potential core of the jet where we expect a constant convective velocity U_c and some aspects of self-similar behavior. Specifically we expect that the axial extent of the wavepacket envelope (or coherence length scale) will be inversely proportional to the frequency ω, or wavenumber $\alpha=\omega/U_c$. Whereas in the original formulation of $p_0(x)$ in Eq.1 we imposed a variation

$$p_0(x) = A(x)e^{i\alpha x}$$

now we are stating

$$p_0(x) = A(\alpha x)e^{i\alpha x}$$

In other words, we replace $p_0(x)$ by the self-similar form $P_0(\alpha x)= P_0(\omega x/U_c)$. Besides its physical basis, this formulation helps clarify the salient variables in the propagation process. In turn, this allows an identification scheme for the dominant azimuthal mode n as a function of frequency ω, a key step towards developing a model that can be applied for all frequencies at once. In the elementary wavepacket analysis of Section II.A, the pressure on the cylinder $r=r_0$ was prescribed as

$$p_w(n, r_0, x, \varphi, t) = p_0(x)e^{-i\omega t+in\phi}$$

We now revise this formulation as follows:

$$p_w(r_0, x, \varphi, t) = \varepsilon(\omega)P_0(\omega x / U_c)e^{-i\omega t+in(\omega)\phi} \tag{13}$$

where $\varepsilon(\omega)$ is an empirically-determined amplitude and the azimuthal mode follows a given relationship with frequency, $n=n(\omega)$. The function $P_0(\omega x/U_c)$ is implied to be a universal function for a given jet. It is easy to show that

$$\hat{p}_0(k) = U_c \frac{\varepsilon(\omega)}{\omega} \hat{P}_0(kU_c / \omega) \tag{14}$$

Considering the far-field solution for the simple wavepacket, the pressure (Eq.5) takes the form

$$p_{w,far} = \varepsilon(\omega)\frac{U_c}{i\omega\pi R}\frac{\hat{P}_0\left(M_c\cos\theta\right)}{H^{(1)}_{n(\omega)}\left(\frac{\omega}{a_\infty}r_0\sin\theta\right)}e^{i\omega R/a_\infty}e^{-i\omega t+in(\omega)\phi} \tag{15}$$

and the intensity (Eq.6) becomes

$$S_{w,far}(R,\theta,\omega) = U_c^2\frac{\varepsilon^2(\omega)}{(\pi R\omega)^2}\left|\frac{\hat{P}_0\left(M_c\cos\theta\right)}{H^{(1)}_{n(\omega)}\left(\frac{\omega}{a_\infty}r_0\sin\theta\right)}\right|^2 \tag{16}$$

where $M_c=U_c/a_\infty$ is the convective Mach number, which is a constant for the shear layers surrounding the potential core of the jet. In Eq.16 the only coupling between frequency and polar angle comes from the Hankel-function term in the denominator. This has important implications on the determination of the azimuthal mode and on the dependence of the spectrum on polar angle for the stochastic version of this model.

Using the same manipulations we readily derive an expression for the far-field intensity of the self-similar wavepacket with azimuthal intensity variation:

$$S_{w,far}(R,\theta,\varphi,\omega) = U_c^2\frac{\varepsilon^2(\omega)}{(\pi R\omega)^2}\left|\hat{p}_0\left(M_c\cos\theta\right)\right|^2\left|\sum_{m=-\infty}^{\infty}\frac{g_m e^{-i|m|\frac{\pi}{2}}}{H^{(1)}_{|m|}\left(\frac{\omega}{a_\infty}r_0\sin\theta\right)}e^{im\phi}\right|^2 \tag{17}$$

The effect of the azimuthal mode $n(\omega)$ is implicit in the values of the Fourier coefficients g_m which now depend on frequency ω. For example, for a Gaussian azimuthal amplitude variation with helical mode n=5, the dominant coefficient in the Fourier expansion will be g_m=5.

D. Combination with Monopole

The wavepacket model by itself may be unable to capture the directivity of jet noise at large polar angles from the jet axis. It is therefore necessary to combine it with a secondary noise source that has omnidirectional character. This source may represent localized sources, near the nozzle exit, that cannot be characterized by a traveling wave. This secondary noise source is selected here to be a monopole with acoustic field

$$p_m(R,t) = \frac{Q}{R} e^{-i\omega t + ikR} \tag{18}$$

where Q denotes the monopole strength. The wavepacket and monopole sources are taken to be uncorrelated to each other, so the intensity of the combined field is the summation of the individual intensities. The modeled intensity in the far field thus takes the form:

$$S_{\text{mod}} = S_{w,far} + \frac{Q^2}{R^2} \tag{19}$$

where $S_{w,far}$ can be given by any of Eqs. 6, 12, 16, or 17. For the jets considered in this study, the monopole intensity is a small fraction of the total intensity.

III. Stochastic Source Model

The actual jet noise source is, of course, random. The stochastic nature of the jet noise source is addressed, at an elementary level, in two steps. First, we consider the pressure on the cylinder surface (Fig.1) to be the superposition of uncorrelated self-similar wavepackets, each wavepacket having full azimuthal coherence. Second, we develop a formulation for a wavepacket that is deterministic axially but has limited azimuthal coherence. The two concepts can be combined into a full stochastic model; however this paper is limited in examining each concept separately, with emphasis on the superposition of self-similar wavepackets.

A. Self-Similar Wavepacket

We construct a stochastic extension of the self-similar wavepacket with uniform azimuthal amplitude. In the analysis that follows, the brackets < > denote the expected value (ensemble average). We envision the pressure perturbation on the cylinder r=r_0 consisting of a superposition of self-similar wavepackets at a spectrum of frequencies:

$$p(x,r_0,\varphi,t) = \int_{-\infty}^{\infty} \varepsilon(\omega)\, P_0\left(\frac{\omega\left(x-\xi(\omega)\right)}{U_c}\right) \exp\left[-i\omega t + in(\omega)\phi\right] d\omega \tag{20}$$

Each elemental wavepacket has random complex amplitude $\varepsilon(\omega)$ and random origin $\xi(\omega)$. The azimuthal mode is a deterministic function of frequency and, as assumed previously, the function $P_0(x)$ is a universal function for a given jet. In the model of Eq.20 we consider only one azimuthal mode at each frequency, whereas in reality the pressure perturbation may contain a series of modes. The wavepackets are mutually uncorrelated, $< \varepsilon(\omega_1)\, \varepsilon(\omega_2) >= 0$ for $\omega_1 \neq \omega_2$.

Since we are interested in the far field ($|\xi| << R$), and there is no interference between any of the wavepackets, their axial origins ξ are irrelevant and we do not need to address them (this would not be true if we were to construct a solution for the near field). A full stochastic model would include a probability distribution for $\xi(\omega)$. Knowing the solution for each individual contribution to the integral from Eq.15, we construct the solution for the far field pressure:

$$p(R,\theta,\phi,t) = -i\int_{-\infty}^{\infty}\varepsilon(\omega)\ \frac{U_c}{\pi R\omega}\frac{\hat{P}_0\left(M_c\cos\theta\right)}{H^{(1)}_{n(\omega)}\left(\dfrac{\omega}{a_\infty}r_0\sin\theta\right)}\ e^{i\omega R/a_\infty}e^{-i\omega t+in(\omega)\phi}d\omega \tag{21}$$

Denoting for convenience

$$\Psi(\omega,\theta) = \frac{U_c}{\pi R\omega}\frac{\hat{P}_0\left(M_c\cos\theta\right)}{H^{(1)}_{n(\omega)}\left(\dfrac{\omega}{a_\infty}r_0\sin\theta\right)} \tag{22}$$

the far field intensity is

$$\left\langle pp^*\right\rangle = \int_{-\infty}^{\infty}\int_{-\infty}^{\infty}\left\langle\varepsilon(\omega)\,\varepsilon^*(\omega')\right\rangle\Psi(\theta,\omega)\Psi^*(\theta,\omega')e^{-i(\omega-\omega')(t-R/a_\infty)}e^{i[n(\omega)-n(\omega')]\phi}d\omega d\omega' \tag{23}$$

where * denotes the complex conjugate. Invoking the orthogonality of the wavepackets in the form

$$\left\langle\varepsilon(\omega)\,\varepsilon^*(\omega')\right\rangle = \frac{E(\omega)}{2\pi}\delta(\omega-\omega'), \tag{24}$$

with $E(\omega)$ being an empirical function and δ the Dirac delta function, the far field intensity becomes

$$\left\langle pp^*\right\rangle = \frac{1}{2\pi}\int_{-\infty}^{\infty}E(\omega)\left|\Psi(\theta,\omega)\right|^2 d\omega \tag{25}$$

Recognizing the integrand as the spectral density (Parseval's theorem),

$$S_w(R,\theta,\omega) = E(\omega)\left|\Psi(\theta,\omega)\right|^2 = U_c^2\frac{E(\omega)}{(\pi R\omega)^2}\left|\frac{\hat{P}_0\left(M_c\cos\theta\right)}{H^{(1)}_{n(\omega)}\left(\dfrac{\omega}{a_\infty}r_0\sin\theta\right)}\right|^2 \tag{26}$$

we obtain essentially the same result as for the deterministic solution, Eq. 16. We note again that the coupling of frequency and polar angle comes solely from the Hankel-function term in the denominator.

B. Superposition of Uncorrelated Azimuthal Disturbances

There is strong experimental evidence that at high frequency the jet turbulence is weakly correlated in the azimuth angle[12], hence the interest in treating azimuthally-incoherent disturbances. Here we are interested in obtaining the far-field solution for a superposition of azimuthally-uncorrelated disturbances. Figure 7 helps illustrate the physics of this problem. A single isolated azimuthal disturbance of extent $\Delta\phi$ creates a far-field intensity distribution (in a given polar direction) that has a certain directivity in ϕ, with extent much wider than $\Delta\phi$. The superposition of isolated azimuthal disturbances, spaced apart by $\Delta\phi$ and covering the whole circle, will lead to a far-field intensity distribution that is the summation of the intensities from each isolated disturbance. Even though the far-field intensity distribution will be uniform in ϕ, the solution to this problem is different from the uniform intensity distribution resulting from the coherent wavepacket of Eq. 6.

For a wavepacket with azimuthal extent $\Delta\phi$ (for example, Gaussian or square-window distributions, as given by Eq. 10) and oriented at azimuth angle ϕ_k, the far-field intensity (Eq.12) can be expressed as

$$S_{w,far}(R,\theta,\varphi,\omega)=\frac{1}{(\pi R)^2}\left|\hat{p}_0\left(\frac{\omega}{a_\infty}\cos\theta\right)\right|^2\Phi(\varphi-\varphi_k,\Delta\varphi,\theta)$$

$$\Phi(\varphi-\varphi_k,\Delta\varphi,\theta)=\left|\sum_{m=-\infty}^{\infty}\frac{g_m e^{-i|m|\frac{\pi}{2}}}{H^{(1)}_{|m|}\left(\frac{\omega}{a_\infty}r_0\sin\theta\right)}e^{im(\varphi-\varphi_k)}\right|^2 \tag{27}$$

Consider now a number of azimuthally-uncorrelated wavepackets according to the middle drawing of Fig.7. The resulting far-field intensity distribution is

$$S_{w,far}(R,\theta,\varphi,\omega)=\frac{1}{(\pi R)^2}\left|\hat{p}_0\left(\frac{\omega}{a_\infty}\cos\theta\right)\right|^2\sum_{k=0}^{K}\Phi(\varphi-\varphi_k,\Delta\varphi,\theta)$$

$$\varphi_k=k\Delta\varphi \tag{28}$$

$$K=\frac{2\pi}{\Delta\varphi}-1$$

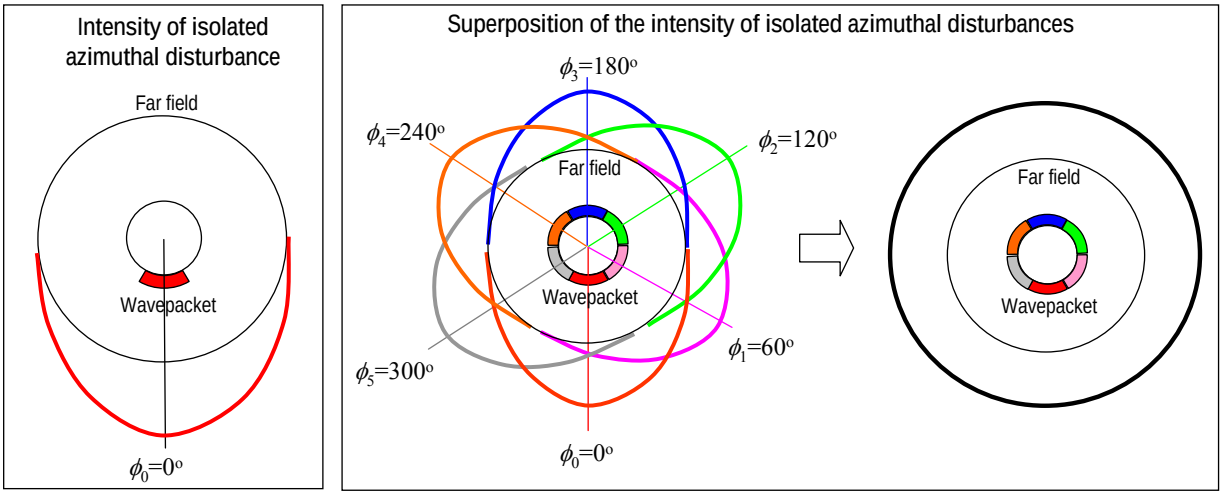

Fig. 7 Illustration of the treatment of azimuthally-uncorrelated wavepackets. In this example the azimuthal spacing is $\Delta\phi$=60°.

If we were to apply the superposition of azimuthally-uncorrelated disturbances to the self-similar wavepacket of Section II.C (i.e., assuming that for each frequency we have a superposition illustrated by Fig.7), the resulting expression for the far-field spectrum becomes

$$S_{w,far}(R,\theta,\omega)=U_c^2\frac{E(\omega)}{(\pi R\omega)^2}\left|\hat{p}_0\left(M_c\cos\theta\right)\right|^2\sum_{k=0}^{K}\Phi(\varphi-\varphi_k,\Delta\varphi(\omega),\theta)$$

$$\varphi_k=k\Delta\varphi \tag{29}$$

$$K=\frac{2\pi}{\Delta\varphi}-1$$

with Φ defined in Eq. 27. A significant complication is that the azimuthal coherence is a function of frequency, $\Delta\phi=\Delta\phi(\omega)$, a relation that is not well established experimentally. Once again, the effect of

azimuthal mode n is implicit in the Fourier coefficients g_m of Eq. 8 and is expected to play a similar role as in the wavepacket with full azimuthal coherence.

C. Combination with Monopole

Considering a monopole of random real strength $q(\omega)$ such that

$$\left\langle q(\omega)\, q(\omega')\right\rangle = \frac{Q(\omega)}{2\pi}\delta(\omega-\omega'), \tag{30}$$

and assuming that the monopole is uncorrelated with the wavepacket, it is evident that the combined spectral density is

$$S_{\text{mod}}(\omega) = S_{w,far}(\omega) + \frac{Q^2(\omega)}{R^2} \tag{31}$$

thus recovering the form of Eq.19.

IV. Source Model Parameterization

The noise source parameterization is based solely on far-field intensity data, such as the spectrum of Fig.1. This is necessitated by the practical consideration the vast majority of experimental studies on jet noise have produced only intensity data. Even though such an approach may seem limited, there are features of the noise spectrum that have not been exploited before that give significant guidance for characterizing the noise source. Two parameterization schemes are presented. The first scheme involves parameterization at fixed frequency and is primarily applicable to the deterministic noise model, although it can also be seen as an elementary building block for the stochastic model. The second, so-called global scheme involves parameterization at all frequencies; it is applicable to both the deterministic model and its stochastic counterpart.

A. Parameterization at Fixed Frequency

Approach

Upon selecting a functional form for the wavepacket shape $p_0(x)$ in Eq.1, the wavepacket shape for given frequency ω and azimuthal mode n can be expressed as

$$p_0(x, A_k)$$

where A_k, k=1,..,K-1, is a vector consisting of K-1 parameters that define the wavepacket shape. The K^{th} parameter is reserved for the monopole strength Q. The parameterization is conducted for a fixed frequency ω and distance R. Having selected a set of parameters, the modeled far-field intensity is given by Eq. 19. The idea is then to select the parameter vector A_k in a way that minimizes the difference between the modeled intensity distribution $S_{\text{mod}}(\theta, n, A_k)$ and the experimental intensity distribution $S_{\text{exp}}(\theta)$. Realizing that we are interested in matching the *shape* (directivity) of the polar intensity distribution, and not so much its absolute value, we work with the normalized values of the modeled and experimental intensities:

$$\begin{aligned}\overline{S}_{\text{mod}}(\theta, n, A_k) &= \frac{S_{\text{mod}}(\theta, n, A_k)}{S_{\text{mod,max}}(n, A_k)}\\ \overline{S}_{\text{exp}}(\theta) &= \frac{S_{\text{exp}}(\theta)}{S_{\text{exp,max}}}\end{aligned} \tag{32}$$

where max denotes the peak value of the polar distribution. The above normalization eliminates the amplitude constant from the minimization process. Once the shape is matched, the absolute levels can be matched through a trivial adjustment of the amplitude. Figure 8 illustrates the minimization process.

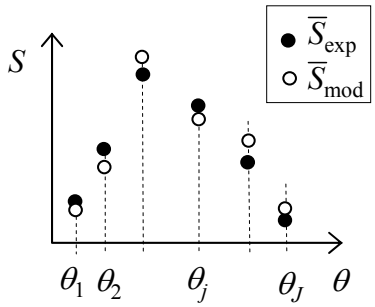

Fig. 8 Illustration of the minimization scheme between modeled and experimental intensity distributions.

Cost function

For a given jet flow, the experimental intensity distribution (autospectrum) is known at discrete polar angles θ_j, j=1,..,J. We construct a cost function based on the relative difference between the modeled and experimental intensity distributions at all the measurement polar angles,

$$F(A_k) = \frac{1}{J}\sum_{j=1}^{J}\left|\frac{\overline{S}_{\exp}(\theta_j) - \overline{S}_{\mathrm{mod}}(n, A_k, \theta_j)}{\overline{S}_{\exp}(\theta_j)}\right|^2 \tag{33}$$

We then seek determination of A_k that minimizes the cost function. However, indiscriminate use of Eq.33 can easily lead to non-physical outcomes for A_k. It is typically necessary to constrain key parameters of the problem to ranges that are physically meaningful. Supposing that we want to constraint the parameters A_k to be near a target value $A_{k,\,\mathrm{target}}$, we add a corresponding penalty to the cost function:

$$F(A_k) = \frac{1}{J}\sum_{j=1}^{J}\left|\frac{\overline{S}_{\exp}(\theta_j) - \overline{S}_{\mathrm{mod}}(m, A_k, \theta_j)}{\overline{S}_{\exp}(\theta_j)}\right|^2 + \sum_{k=1}^{K} C_k\left(A_k - A_{k,\mathrm{target}}\right)^2 \tag{34}$$

where C_k is a vector of appropriately chosen penalty coefficients.

In this study the wavepacket axial shape is assigned the form

$$p_0(x) = \tanh(x/b_1)^{p_1}\left\{1 - \tanh(x/b_2)^{p_2}\right\}e^{i\alpha x} \tag{35}$$

which was selected as a promising function based on earlier work[11]. The amplification is controlled by the length scale b_1 and power p_1, and the decay is controlled by length scale b_2 and power p_2. The noise source parameter vector is defined as:

$$\begin{aligned} A_1 &= \frac{U_c}{U_j} = \frac{\omega/\alpha}{U_j} \\ A_2 &= b_1 \\ A_3 &= b_2 \\ A_4 &= p_1 \\ A_5 &= p_2 \\ A_6 &= Q \end{aligned} \tag{36}$$

Constraints are placed on A_1 so that the convective velocity U_c is close to a target value of about $0.6U_j$. The wavenumber α is thus determined from the parameter A_1. The minimization process of Eq.34 used the Restarted Conjugate Gradient method of Shanno and Phua[13] (ACM TOM Algorithm 500).

Results for Mach 0.9 jet

The jet in this investigation was cold with Mach number M_j=0.9, velocity U_j=285 m/s, and diameter D_j=21.8 mm. Parameterization of the wavepacket requires judicious choices for the azimuthal mode and a reasonable constraint for the convective velocity ratio U_c/U_j. Experimentation with the minimization

process of Eq. 34 shows that, for given frequency, there are one or two azimuthal modes that can fit the experimental results very well, while for other modes it is impossible to get a good fit regardless of the parameter values. For example, for Sr=0.2 mode n=0 works best; for Sr=0.5, n=1; and for Sr=1.0, n=3. The predominance of modes n=0,1,2, and 3 for this range of Strouhal numbers is in line with results of azimuthal microphone measurements on similar jets by Juve *et al.*[14] and by Brown and Bridges[15]. In general, it is found that a higher azimuthal mode is needed with increasing frequency.

The other consideration is the convective velocity ratio U_c/U_j, which here is set to range between 0.45 (low frequency) to 0.6 (high frequency). As mentioned before, U_c/U_j was the only constraint in the cost function. Figures 9, 10, and 11 show parameterization results for Strouhal numbers Sr=0.2, 0.5, and 1.0, respectively. Plotted are the wavepacket shape $p_0(x)$ and the modeled and experimental intensity distributions. With increasing frequency, the minimization scheme leads to smaller wavepacket widths, which makes physical sense. Note the increasing azimuthal mode with higher frequency. Figures 9-11 demonstrate that good fits can be obtained between the modeled and experimental intensity polar distributions, with errors of less than about 10% in the square root of the cost function of Eq. 34.

Figure 12 depicts the parameterization of a wavepacket at Sr=1 with azimuthal coherence of 30 deg, using the intensity formulation of Eq. 28. The wavepacket is moderately longer than the one found for the fully-coherent case of Fig. 11. Again, azimuthal mode n=3 was needed to get a good match between modeled and experimental directivities.

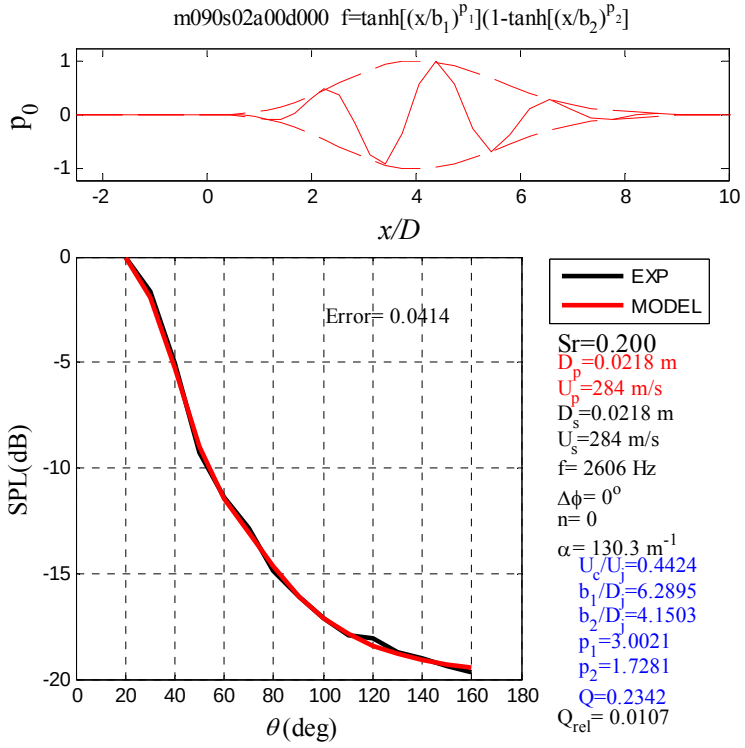

Fig. 9 Parameterization for Mach 0.9 cold jet at Sr=0.2. Azimuthal mode n=0.

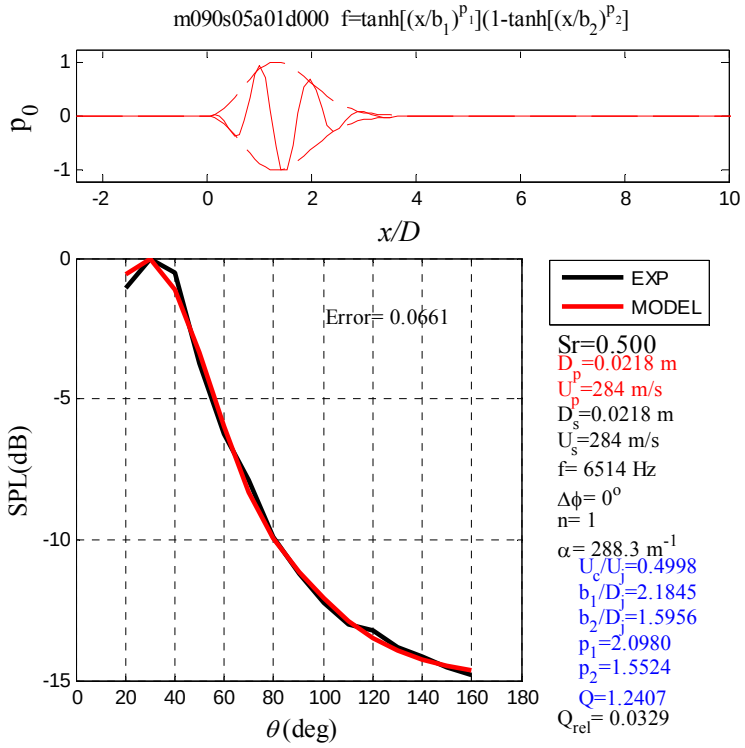

Fig. 10 Parameterization for Mach 0.9 cold jet at *Sr*=0.5. Azimuthal mode *n*=1.

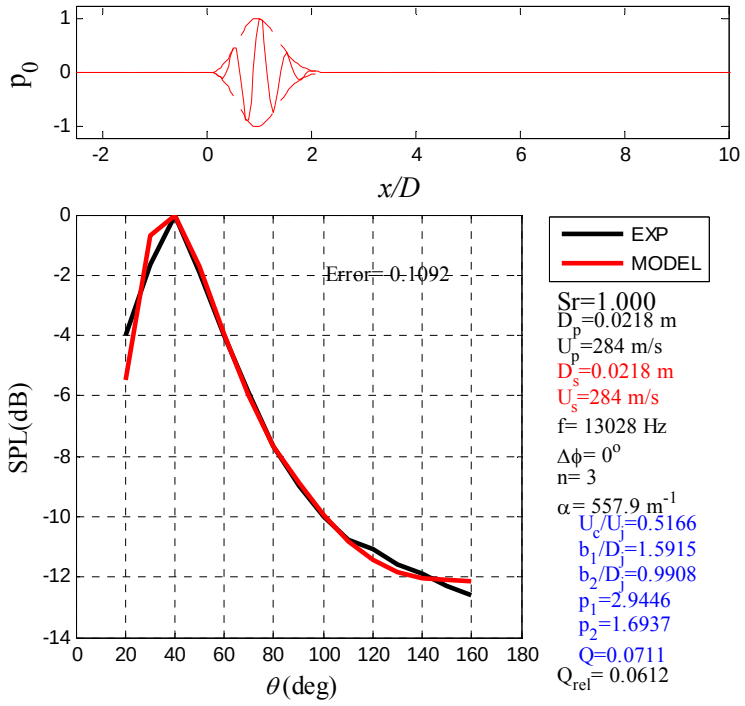

Fig. 11 Parameterization for Mach 0.9 cold jet at *Sr*=1.0. Azimuthal mode *n*=3.

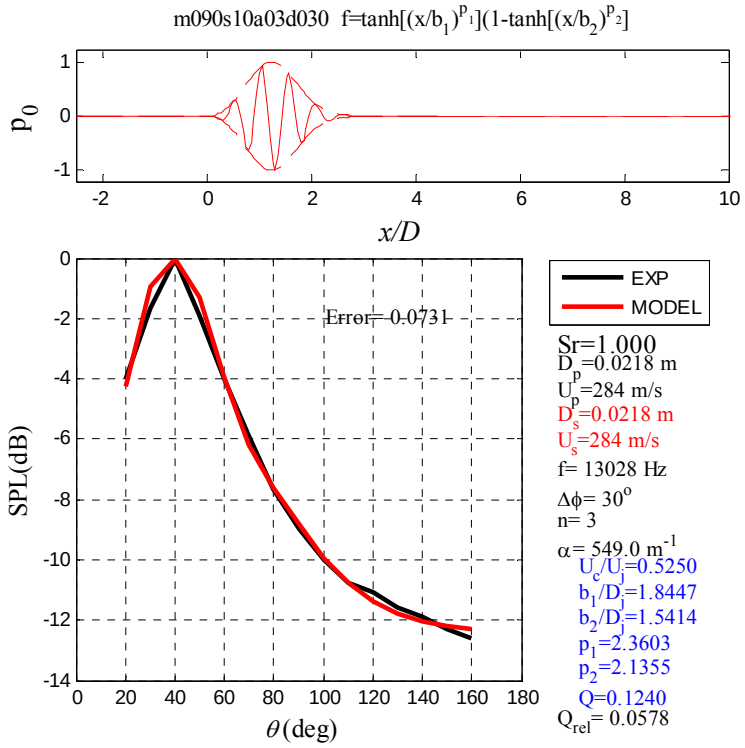

Fig. 12 Parameterization for Mach 0.9 cold jet with 30-deg azimuthal coherence at *Sr*=1.0. Azimuthal mode *n*=3.

B. Global Parameterization

Approach

The preceding methods dealt with determination of the noise source parameters for a given frequency. The global parameterization procedure pertains to estimating the source parameters at all frequencies of interest using a single minimization scheme. It is based on prescription of general trends versus frequency for the wavepacket and monopole parameters. In this paper it is applicable only to the wavepacket model with full azimuthal coherence. Central to this scheme is the *self-similar* wavepacket formulation of Section II.C.

The source parameters A_k remain as defined in Eq.36. Now, however, they are given as functions of frequency ω, using the relations below and the parameter vector B_k

$$
\begin{aligned}
A_1 &= \frac{U_c}{U_j} = \frac{\omega/\alpha}{U_j} = B_1 \tanh(B_2 \omega^{0.3}) \\
A_2 &= \frac{b_1}{D_j} = \frac{B_3}{\omega} \\
A_3 &= \frac{b_2}{D_j} = \frac{B_4}{\omega} \\
A_4 &= p_1 = B_5 + \frac{B_6}{\omega^2} \\
A_5 &= p_2 = B_7 + \frac{B_8}{\omega^2} \\
A_6 &= Q = B_9 \tanh(B_{10}\omega)
\end{aligned}
\tag{37}
$$

The tanh trend for the convective velocity (A_1) comes from the expectation that at low frequency (typically Strouhal numbers less than 0.1) noise comes from the region past the potential core where the velocity (and consequently the ratio U_c/U_j) decays. As the frequency increases, the noise source location tends toward the potential-core region where the $U_c \approx$ constant. The expressions for the widths (A_2, A_3) are consistent with the self-similar concept of the wavepacket where the width is inversely proportional to frequency. The exponents (A_4, A_5) depend on frequency only for low frequencies where we are dealing with flow past the potential core. Finally, the monopole strength (A_6) displays a tanh trend with frequency based on experience using the standard parameterization approach.

Azimuthal mode versus frequency

A critical aspect of the global parameterization scheme is a reasonable prescription for the dominant azimuthal mode versus frequency. It was noted earlier that higher modes are required to match the jet directivity with increasing frequency. Here we try to put this observation on a quantitative basis. Refer to the solution for the intensity for the self-similar wavepacket, Eq. 26. The polar direction of peak emission (where $S_{w,\text{far}}$ is maximixed at given frequency) is obtained by differentiating Eq.26 with respect to the polar angle θ, resulting in:

$$
\frac{d}{d\theta} \frac{\left|\hat{P}_0\left(M_c \cos\theta\right)\right|}{\left|H^{(1)}_{n(\omega)}\left(\frac{\omega}{a_\infty} r_0 \sin\theta\right)\right|} = 0 \tag{38}
$$

For a given universal wavepacket funtion $P_0(\xi)$, Eq. 38 gives the direction of peak emission θ_{peak} as a function of frequency ω and azimuthal mode $n(\omega)$. Figure 13 shows such as solution on the polar angle - Strouhal number plane. For each azimuthal mode n, the blue line defines the locus of θ_{peak} versus frequency. Overlayed on the diagram is the experimental direction of peak emission. The intersection of the theoretical curves with the experimental curve define the azimuthal mode number versus frequency. It is seen that as the frequency increases, progressively higher modes are needed to match the experimental directivity. Aside from its practical value, the process illustrated by Fig. 13 indicates a strong connection between azimuthal mode content and directivity of jet noise.

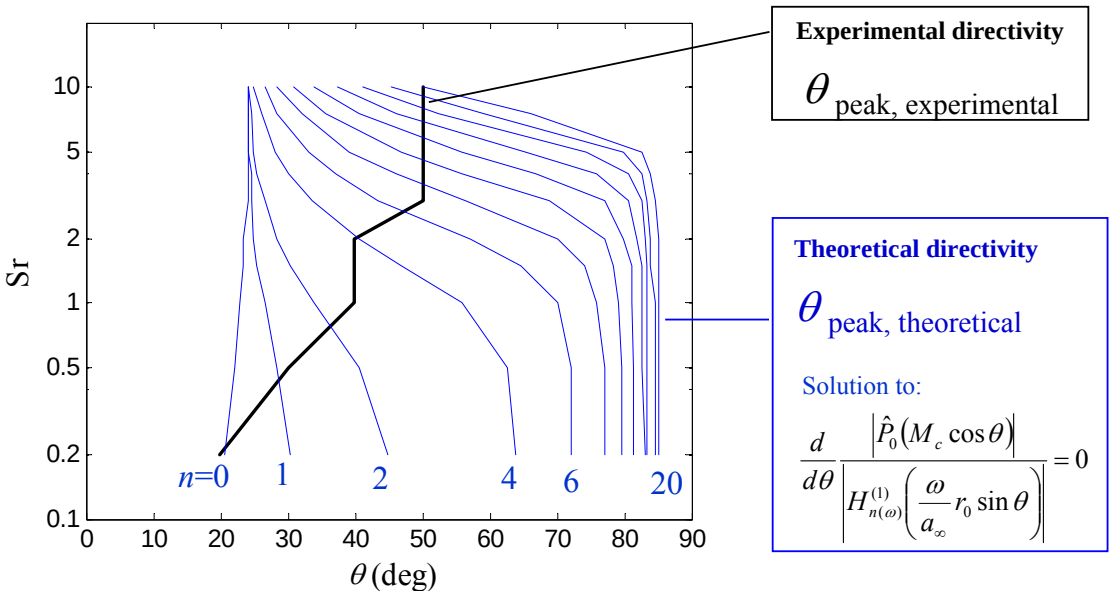

Fig. 13 Determination of azimuthal mode versus frequency.

Cost function

We seek parameters B_k (10 parameters for the scheme of Eq. 37) that minimize the difference, in a least-squared sense, of the modeled and experimental autospectra for all the polar angles and frequencies (Strouhal numbers) of interest. The cost function becomes:

$$F(B_k)=\frac{1}{N_j N_q}\sum_{q=1}^{N_q}\sum_{j=1}^{N_j}\left|\frac{\overline{S}_{\text{exp}}(\theta_j,\omega_q)-\overline{S}_{\text{mod}}(n_q,B_k,\theta_j,\omega_q)}{\overline{S}_{\text{exp}}(\theta_j,\omega_q)}\right|^2 \quad + \quad \sum_{k=1}^{K}C_k\left(B_k-B_{k,\text{target}}\right)^2 \qquad (39)$$

where θ_j, j=1,.., N_j are the polar angles of interest and ω_q, q=1,.., N_q are the frequencies of interest. As with the standard cost function of Eq. 34, we constrain selected parameters to fall within a certain range through the second term in the cost function. In this study only the parameter B_1, governing the convective velocity ratio, was constrained.

To determine the azimuthal modes n_q using the process of Eq. 38, we need a reasonable choice for the universal wavepacket shape $P_0(\xi)$. We determine this shape by applying Eq. 39 at a single frequency - essentially reducing it to Eq. 34. The frequency should be high enough that the self-similar assumption is valid - typically Strouhal number at or above 0.5. We minimize the cost function for a variety of azimuthal modes, and select the mode (and associated model parameters, B_1,..., B_{10}) that provide the best match between modeled and experimental intensities for that frequency. Now that we have the desired wavepacket shape, we apply the azimuthal-mode-determination scheme of Eq. 38. Once the modes are determined, the global minimization process of Eq. 39 is applied for all frequencies of interest.

Results for Mach 0.9 jet

Fig. 14 shows results of a global parameterization of the Mach 0.9 jet, using two conditions. In the first condition, the parameterization was performed for the wavepacket alone, setting the monopole strength to zero. In the second condition, the monopole strength was included in the parameters. Each subfigure depicts contour plots of the experimental and modeled spectra, as well as line plots of the modeled spectrum at polar angles θ=25° and θ=90°.

Examining the predictions for the wavepacket alone, Fig. 14a, we see that the main features of the spectrum are matched but there are quantitative discrepancies in low θ - high Sr corner of the spectrum. The broadening of the spectrum with increasing polar angle is unquestionable. This is very significant. A single noise source -- the wavepacket -- creates a narrow spectrum at small angles and a wide spectrum

at large angles. The spectral change comes from the Hankel function term discussed previously, in conjunction with the azimuthal-mode determination of Eq. 38. Even though this result does not preclude an additional source broadening the spectrum, it shows that a two-source model is not necessary to explain the variation of the spectrum with polar angle.

Including the monopole, Fig. 14b, allows an excellent match between the modeled and experimental spectra. The monopole may represent, in a very simple way, the "incoherent" noise source of the two-source model. Alternatively, it may represent noise source associated with real effects such as reflections from the nozzle lip or nozzle surface. It is clear that addition of the monopole does not change the conclusions of the previous paragraph.

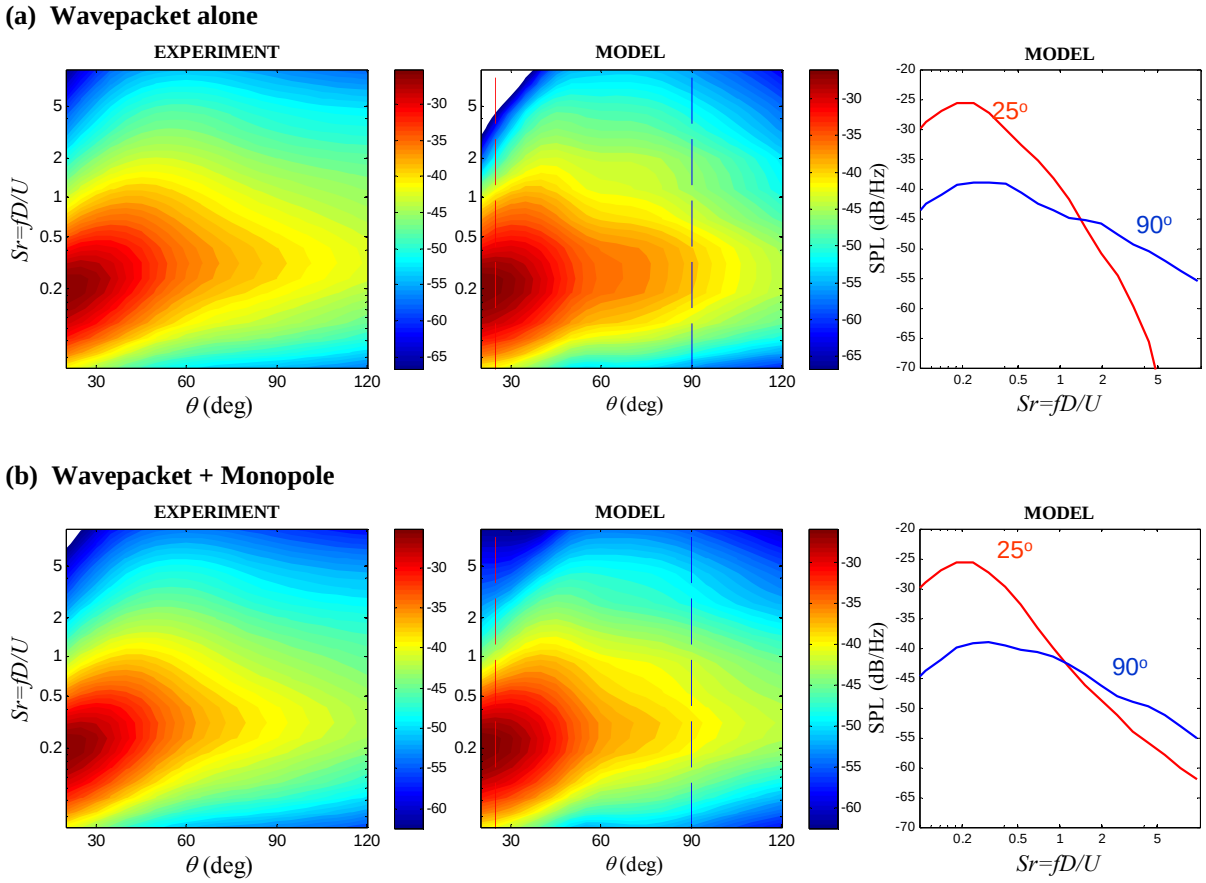

Fig. 14 Results of the global parameterization of a Mach 0.9 cold jets. Contour plots compare the experimental and modeled autospectra.

V. Concluding Remarks

Whereas previous experimental studies have focused on investigating the noise source at a small number of frequencies (typically near the Strouhal number of peak emission), the present study underscores the importance and benefits of looking at the entire spectrum of jet noise as illustrated in Fig.1. In particular, the directivity-versus-frequency trend provides new insights into the azimuthal content of the noise source.

This study demonstrated that a significant amount of information can be inferred from the far-field spectrum, particularly from its directivity, that enables construction of a wavepacket with reasonable physical characteristics. To construct the noise source model for a given frequency, the wavepacket is parameterized and the parameters are determined by least-squares minimization of the difference between the modeled and experimental sound intensity distributions in the far field.

The parameterization process can be applied simultaneously to all frequencies of interest through the concept of the self-similar wavepacket, i.e., a wavepacket with universal shape whose axial scale varies inversely with frequency. A stochastic extension of this concept shows a connection between the shape of the far-field spectrum and the emission polar angle. This relation indicates that the broadening of the spectrum with increasing polar angle can be explained on the basis of a single noise source (the wavepacket), rather than the prevailing model of two disparate noise sources, one coherent and the other incoherent.

The self-similar wavepacket model presented here is a simple formulation that needs to be further extended. The obvious next step is to combine the two stochastic approaches of Section III into a single unified model, namely a wavepacket that is stochastic in both axial and azimuthal directions. A necessity in this physical modeling is knowledge of the azimuthal coherence of the jet - if not of the turbulence itself at least of the near pressure field. Such measurements are critical for our understanding and modeling of jet noise.

Acknowledgment

This research has been funded by Boeing Subcontract No. 208547 in support of NASA contract NNL07AA54C "Acoustic Prediction Methodology and Test Validation for an Efficient Low-Noise Hybrid Wing Body Subsonic Transport."

References

1. Russell, J., and Berton, J., "Stone Jet Noise Module (ST2JET)", ANOPP Theoretical Manual, ver.25, NASA Langley Research Center, Hampton, VA, 2006.
2. C.K.W. Tam, K. Viswanathan, K.K. Ahuja, J. Panda, J., "The sources of Jet Noise: Experimental Evidence", *Journal of Fluid Mechanics*, Vol. 615, 2008, pp. 253-292.
3. Bonnet, C.M.T., and Fisher, J., "Correlation Techniques and Modal Decomposition Analysis for the Detection of Azimuthally Coherent Structures in Jet Flows," *Journal of Sound and Vibration*, Vol. 66, No.4, October 1979, pp.545-555.
4. Papamoschou, D., "Imaging of Distributed Directional Noise Sources," *Journal of Sound and Vibration*, Vol. 330, No.10, 2011, pp. 2265-2280.
5. Tam, C. K. W., and Burton, D. E., "Sound Generation by the Instability Waves of Supersonic Flows. Part 2. Axisymmetric Jets," *Journal of Fluid Mechanics*, Vol. 138, 1984, pp. 273-295.

6. Crighton, D.G. and Huerre, P., "Shear-Layer Pressure Fluctuations and Superdirective Acoustic Sources," *Journal of Fluid Mechanic*s, Vol. 220, 1990, pp. 355-368.

7. Avital, E.J., Sandham, N.D., and Luo, K.H., "Mach Wave Radiation by Mixing Layers. Part I: Analysis of the Sound Field," *Theoretical and Computational Fluid Dynamics*, Vol. 12, 1998, pp. 73-90.

8. Morris, P.J., "A Note on Noise Generation by Large Scale Turbulent Structures in Subsonic and Supersonic Jets," *International Journal of Aeroacoustics*, Vol. 8, No. 4, 2009, pp. 301-316.

9. Reba, J., Simonich, J., and Schlinker, R., "Sound Radiated by Large-Scale Wave-Packets in Subsonic and Supersonic Jets," AIAA Paper 2009-3256, May 2009.

10. Reba, R., Narayanan, S., and Colonius, T., "Wave-Packet Models for Large-Scale Mixing Noise," *International Journal of Aeroacoustics*, Vol. 9, No. 4-5, pp. 533-558, 2010.

11. Papamoschou, D., "Prediction of Jet Noise Shielding," AIAA Paper 2010-0653, Jan. 2010.

12. Sreenivasan, K.R., "The Azimuthal Correlations of Velocity and Temperature Fluctuations in an Axisymmetric Jet," *Physics of Fluids*, Vol. 27, pp. 867-875, 1984.

13. Shanno, D.F., and Phua, K.H., "Minimization of Unconstrained Multivariate Functions," *ACM Transactions on Mathematical Software*, Vol. 6, No.4, 1980, pp. 618-622.

14. Juve, D., Sunyach, M., and Comte-Bellot, G., "Filtered Azimuthal Correlations in the Acoustic Far Field of a Subsonic Jet," *AIAA Journal*, Vol. 17, No.1, 1979, pp. 112-113.

15. Brown, C., and Bridges, J., "Acoustic Efficiency of Azimuthal Modes in Jet Noise Using Chevron Nozzles", AIAA Paper 2006-2654, Jan. 2006.